Supporting Information

Unveiling Dynamic Surface Transformations: Mo-Doped Fe-Based MOFs as Next-Generation Oxygen Evolution Catalysts

Sheraz Muhammad [a], Bowen Yao [a], Aling Zhou [a], Zhiyang Huang [a], Sumayya Khan [a], Fengli Wei [a], Zuyang Luo [a], Tayirjan Taylor Isimjan [b,*], Xiulin Yang [a,*]

[a] *Guangxi Key Laboratory of Low Carbon Energy Materials, School of Chemistry and Pharmaceutical Sciences, Guangxi Normal University, Guilin 541004, China*

[b] *Saudi Arabia Basic Industries Corporation (SABIC) at King Abdullah University of Science and Technology (KAUST), Thuwal 23955-6900, Saudi Arabia*

** Corresponding authors.*

E-mail addresses: isimjant@sabic.com (T.T. Isimjan); xlyang@gxnu.edu.cn (X. Yang).

1. Material characterization

The morphology and microstructure of the as-prepared catalysts were analyzed using advanced electron microscopy techniques, including scanning electron microscopy (SEM, FEI Quantum 200 FEG) and transmission electron microscopy (TEM, JEM-2100F). Crystallographic information was obtained through X-ray powder diffraction (XRD) measurements conducted with a D/Max-3c diffractometer (12 kW, Cu Kα radiation) at a scanning speed of 5° min^{-1}. Fourier-transform infrared (FTIR) spectroscopy was performed using a Thermo Scientific Nicolet iS50 spectrometer and thermogravimetric analysis (TGA) was conducted on a Mettler Toledo TGA/DSC 3+ instrument to investigate functional groups and thermal stability, respectively. The chemical valence states of the elements present in the catalysts were characterized using X-ray photoelectron spectroscopy (XPS, JPS-9010 with Mg Kα radiation).

2. Electrochemical measurements

All electrochemical tests for the catalysts synthesized in this experiment were conducted using a Biologic VMP3 electrochemical workstation, which employs a standard three-electrode system with an electrolyte solution of 1.0 M KOH. The working electrode for electrochemical testing was the prepared NF-based catalyst (1 cm × 1 cm), the counter electrode was a graphite plate, and the reference electrode was a standard calomel electrode (SCE). Linear sweep voltammetry (LSV) was used to measure the electrochemical properties of the catalysts. The scans were conducted in the range of 1.2-0 V (vs. SCE) with a sweep rate of 0.5 mV/s. Electrochemical impedance spectroscopy (EIS) measurements were taken at a voltage of 0.5 V (vs. SCE) over a frequency range of 300 kHz to 10 mHz, with the EIS data fitted using ZSimDemo software. The electrochemical surface area (ECSA) was determined from the double-layer capacitance (C_{dl}), which was obtained through cyclic voltammetry (CV) characterization. The CV measurements

were conducted in the non-Faradaic voltage range of 0.1–0.2 V (vs. SCE) at scan rates of 10, 20, 30, 40, 50, and 60 mV/s^{-1}. The formula for calculating C_{dl} is:

$$C_{dl} = \frac{j_a - j_c}{2 \times v}$$

where j_a and j_c are the anode and cathode current densities, respectively, and ν represents the scan rate. The ECSA was calculated as:

$$ECSA = \frac{C_{dl}}{C_s}$$

where C_s is the specific capacitance, which typically ranges between 20 and 60 μF cm^{-2}, with an average value of 40 μF cm^{-2}. The stability of the catalyst was assessed by chronopotentiometry at current densities of 20 and 100 mA cm^{-2} over an extended time period. The overall water splitting tests were conducted in a 1.0 M KOH electrolyte with potentials ranging from 0 to 2.5 V and a scan rate of 2 mV/s^{-1}. The experimentally measured potentials were converted to the RHE scale using the Nernst equation:

$$E(vs.\,RHE) = S_{SCE} + 0.059 \times pH + 0.241\ V$$

and corrected with 100% *iR* compensation as per the equation. In situ Raman spectroscopy experiments were carried out using a Raman spectrometer (InVia Qontor, Renishaw) equipped with an in-situ test cell (GaossUnion C031-1) for experimentation in 1.0 M KOH solution. The as-prepared catalyst served as the working electrode, with a carbon rod as the counter electrode and an Ag/AgCl electrode as the reference electrode. The laser excitation wavelength was set at 785 nm, and the exposure time for each spectral recording was 10 min. The evolution of the catalyst was monitored by collecting Raman spectra at a constant potential of 1.10-1.5 V (vs. RHE). In situ EIS were performed at different potentials in the frequency range of 0.01-100000 Hz. In-situ attenuated total reflectance (ATR) FTIR measurements were carried out using a three-electrode

setup with the catalyst/glass carbon electrode as the working electrode, an Ag/AgCl electrode as the reference electrode, and a Pt wire as the counter electrode in 1.0 M KOH solution. The in-situ characterization was performed with a FTIR spectrometer (Nicolet 6700, Thermo-Fisher Scientific) equipped with an extended-range diamond ATR accessory. The signals were periodically recorded every 15 s, and the in-situ electrochemical device was controlled by an electrochemical workstation using a chronoamperometry method with applied potentials increasing from 1.0 to 1.8 V vs. RHE.

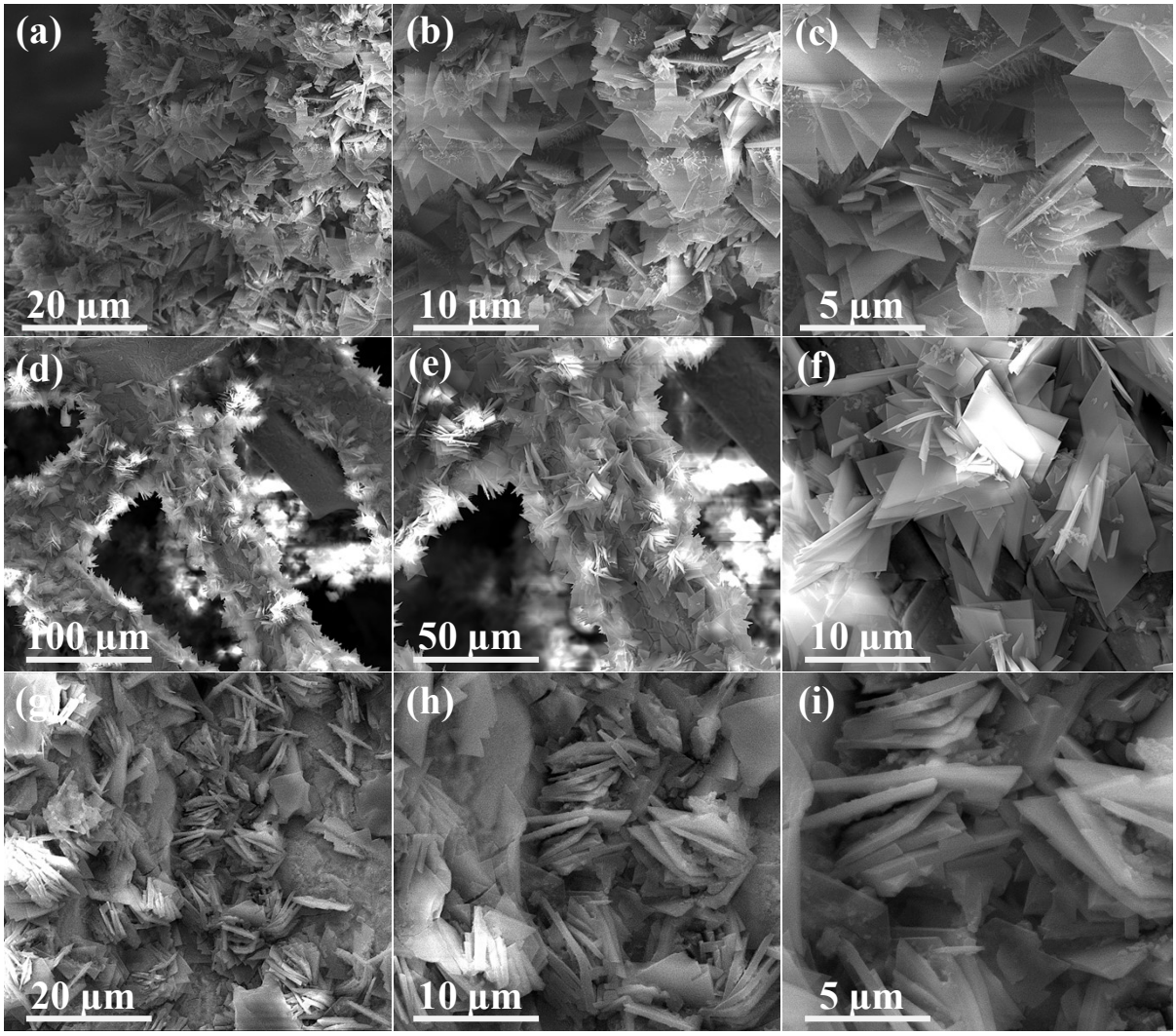

Fig. S1. SEM images of (a-c) $Mo_{0.1}Fe\text{-}NH_2\text{-}BDC$, (d-f) $Mo_{0.2}Fe\text{-}NH_2\text{-}BDC$, and (g-i) $Mo_{0.3}Fe\text{-}NH_2\text{-}BDC$

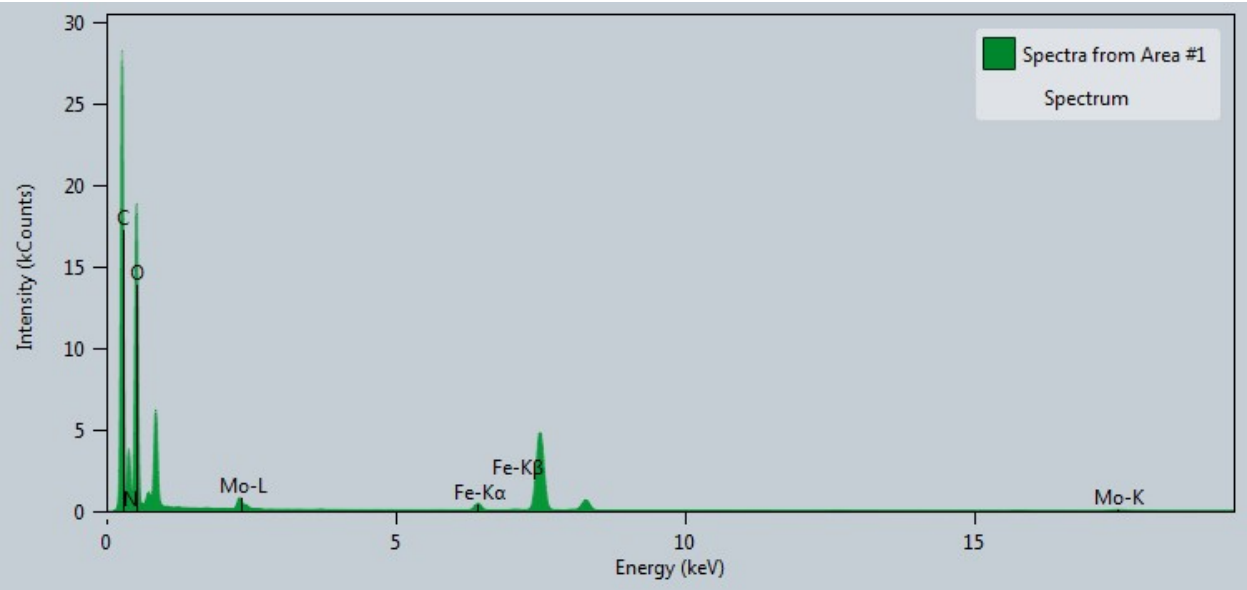

Fig. S2. EDX of $Mo_{0.2}Fe\text{-}NH_2\text{-}BDC$.

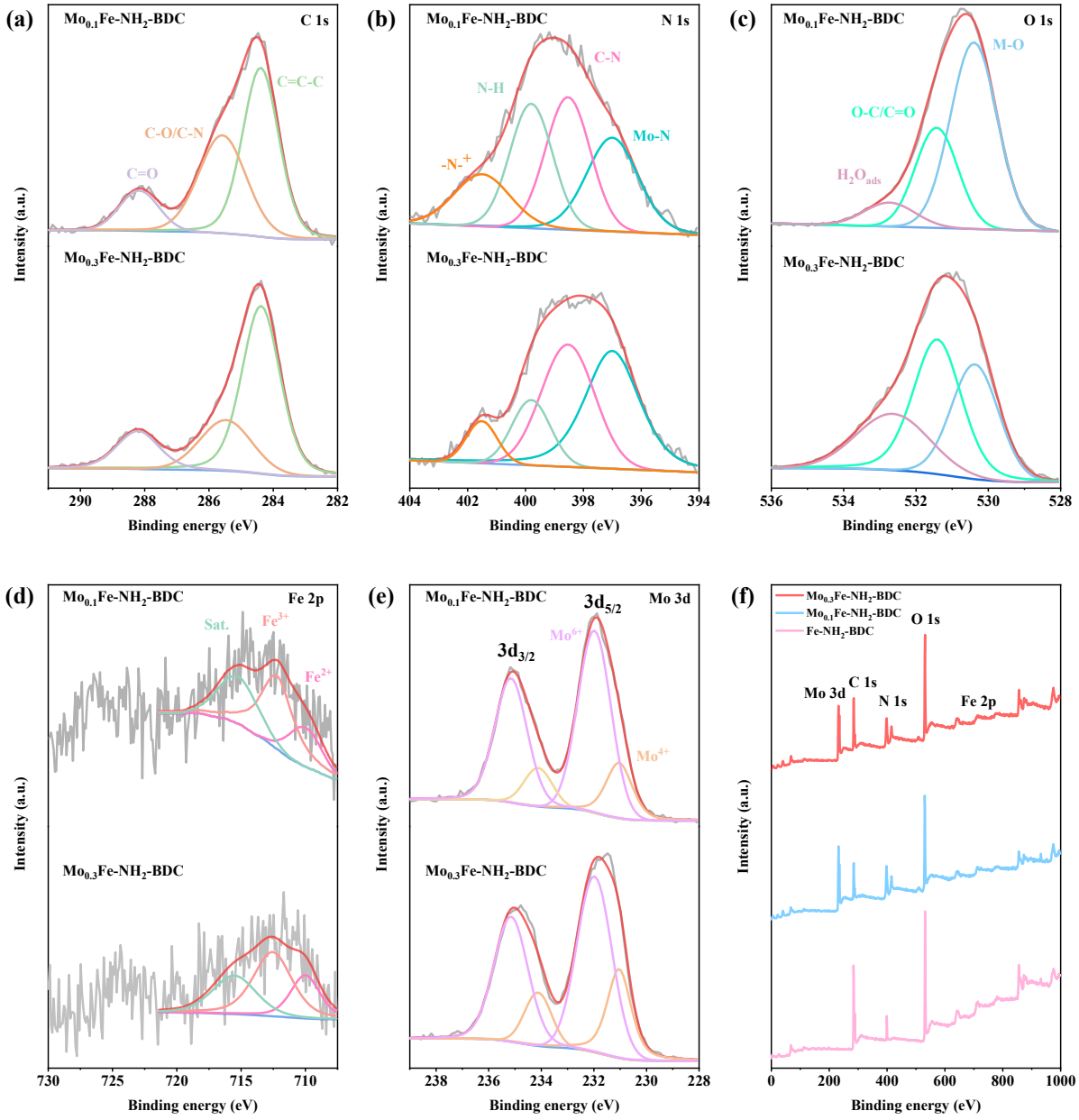

Fig. S3. High-resolution XPS spectra of (a) C 1s, (b) N 1s, (c) O 1s, (d) Fe 2p, (e) Mo 3d, and (f) XPS survey for Fe-NH_2-BDC, $Mo_{0.1}$Fe-NH_2-BDC and $Mo_{0.3}$Fe-NH_2-BDC.

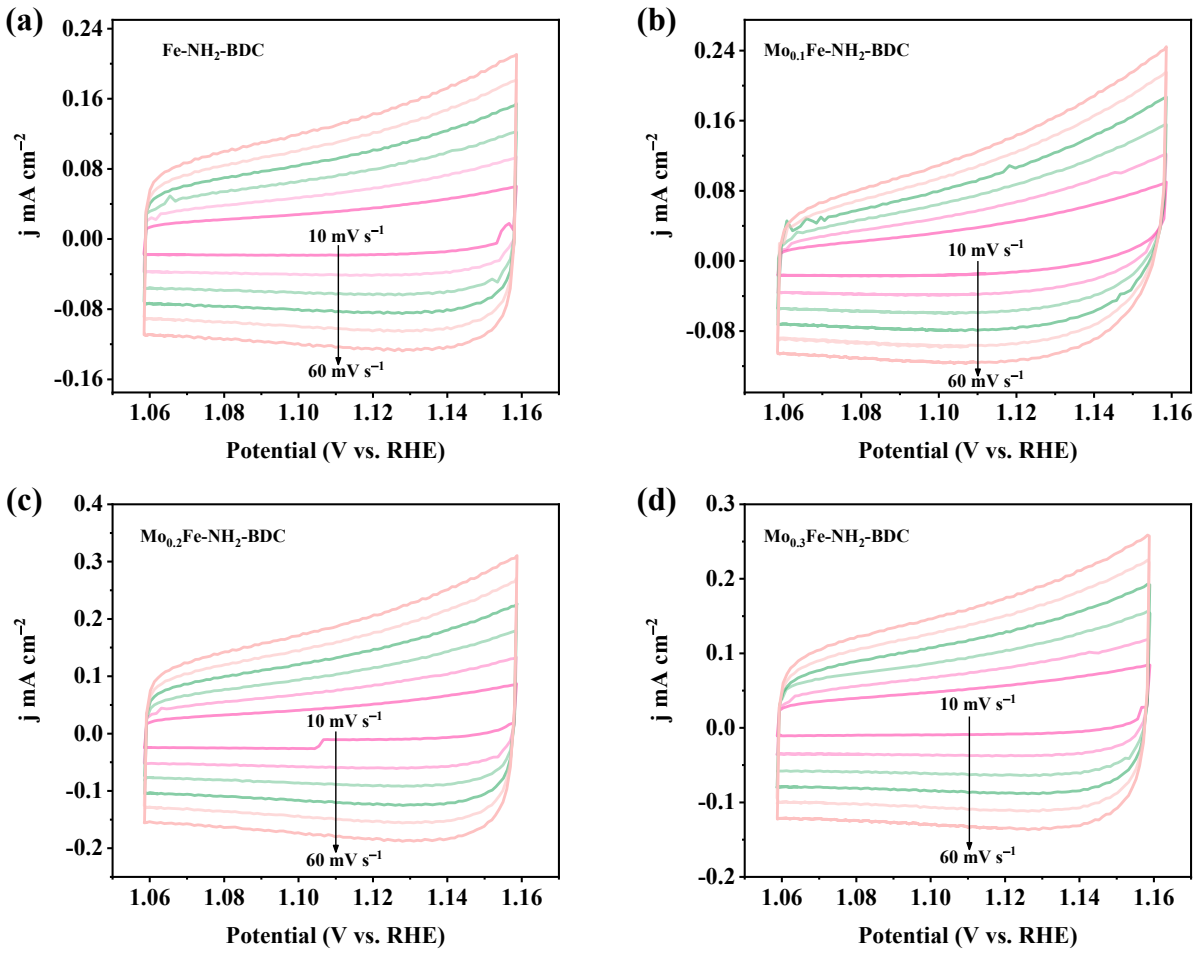

Fig. S4. CV curves of (a) Fe-NH_2-BDC, (b) $Mo_{0.1}$Fe-NH_2-BDC, (c) $Mo_{0.2}$Fe-NH_2-BDC, and (d) $Mo_{0.3}$Fe-NH_2-BDC operated in non-Faradaic potential window with different scan rates (10-60 mV s^{-1}).

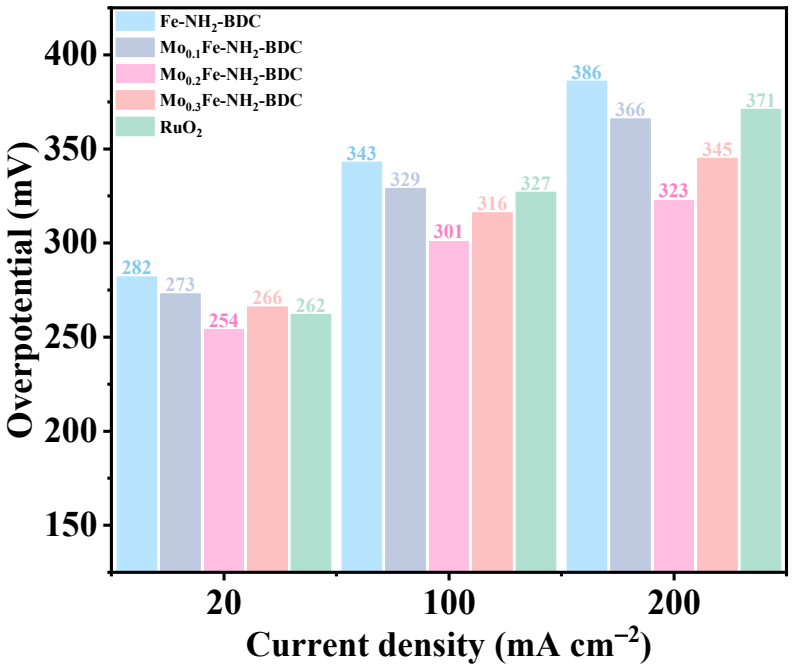

Fig. S5. Overpotential comparison of Fe-NH_2-BDC, Mo_xFe-NH_2-BDC (x = 0.1, 0.2, 0.3), and RuO_2 at 20, 100, and 200 mA cm^{-2}.

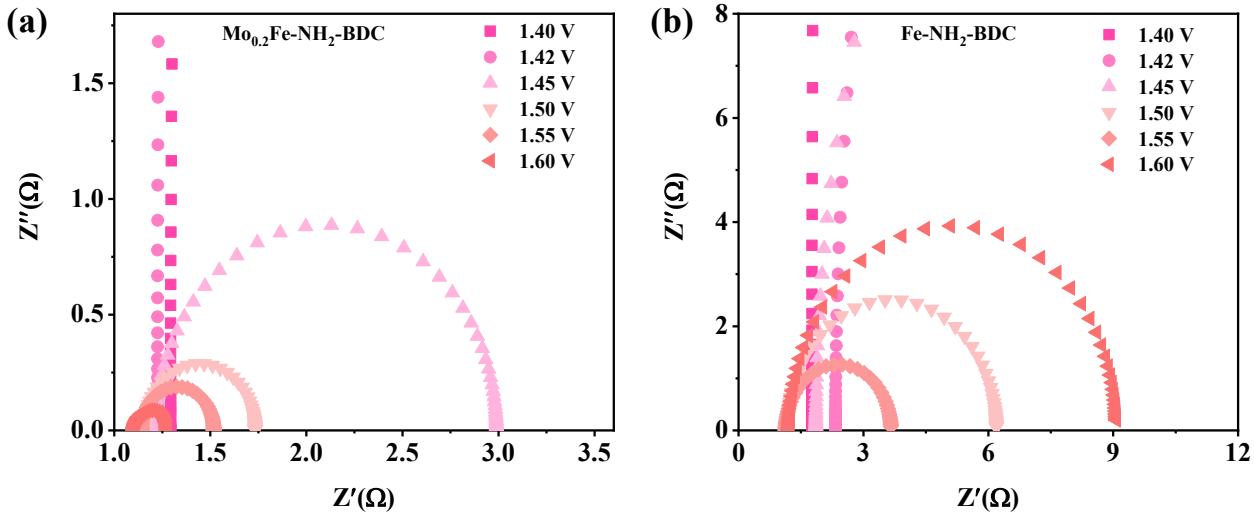

Fig. S6. Nyquist plots for (a) $Mo_{0.2}$Fe-NH_2-BDC and (b) Fe-NH_2-BDC at different applied potentials.

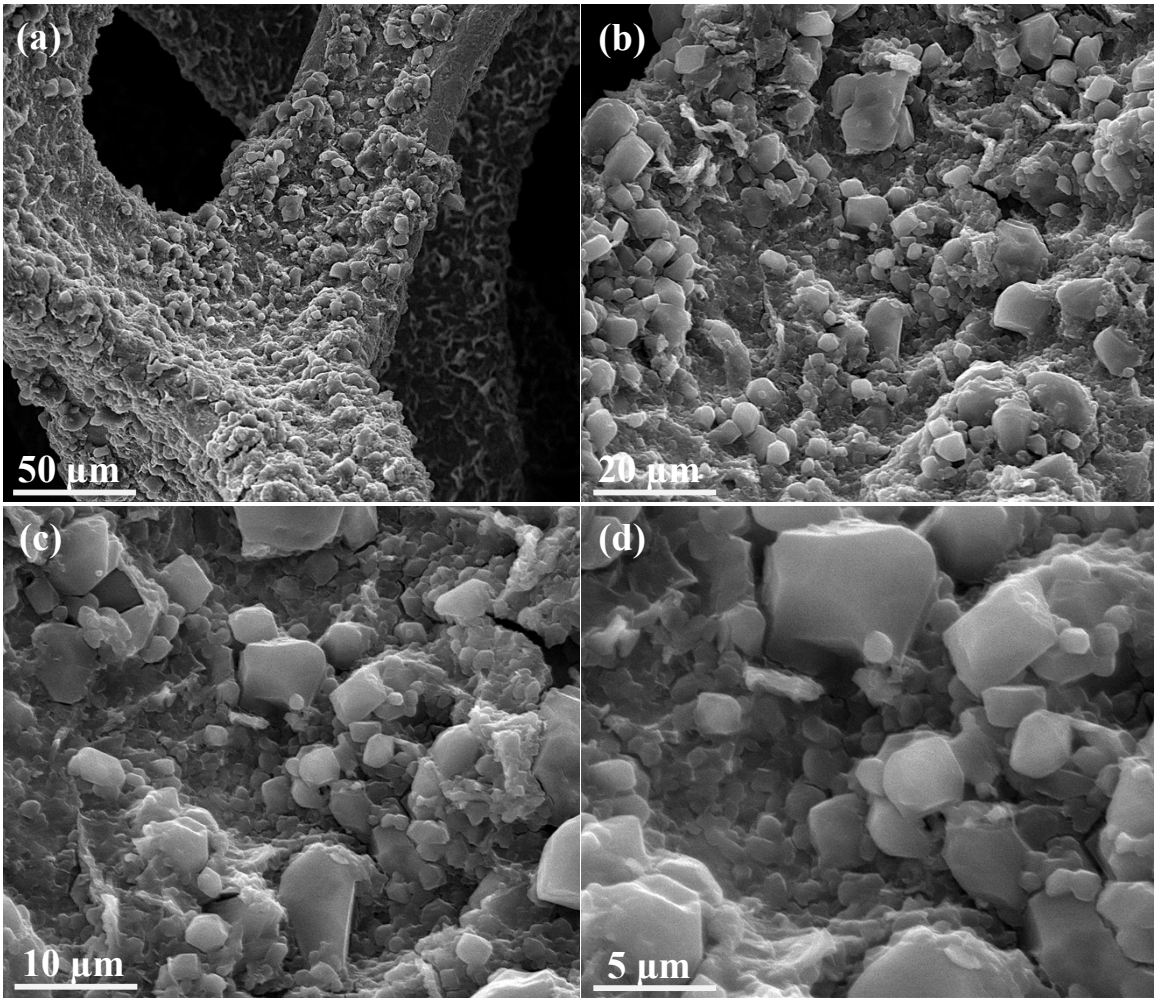

Fig. S7. SEM images of (a-d) $Mo_{0.2}Fe\text{-}NH_2\text{-}BDC$ after OER stability test.

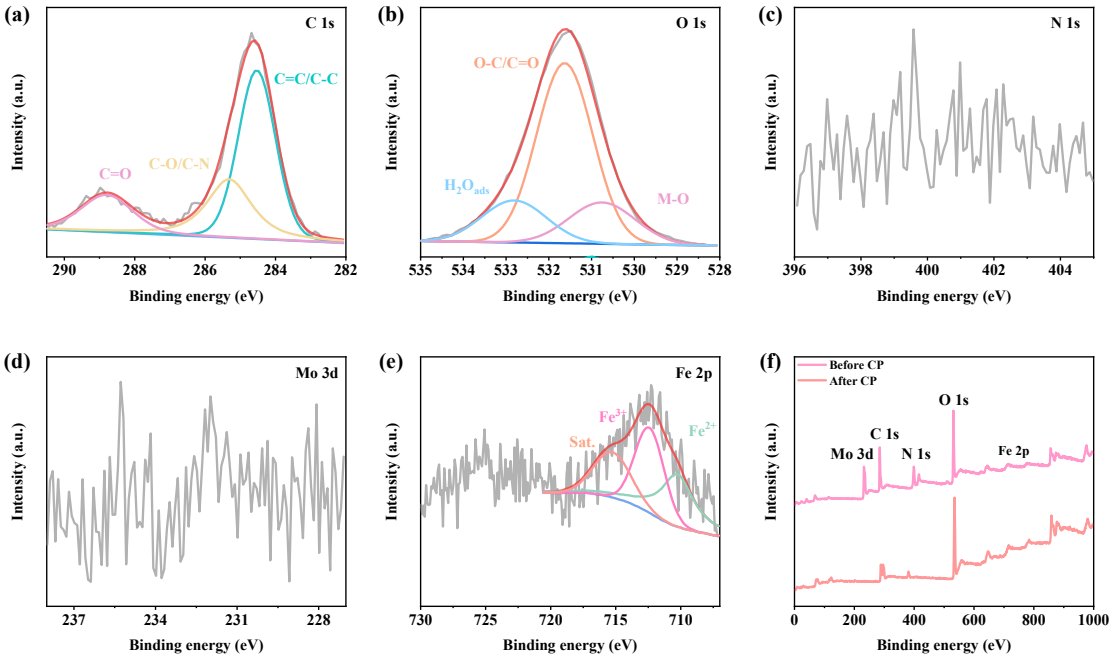

Fig. S8. High-resolution XPS spectra of (a) C 1s, (b) N 1s, (c) O 1s, (d) Fe 2p, (e) Mo 3d, and (f) XPS survey of $Mo_{0.2}Fe\text{-}NH_2\text{-}BDC$ after stability test.

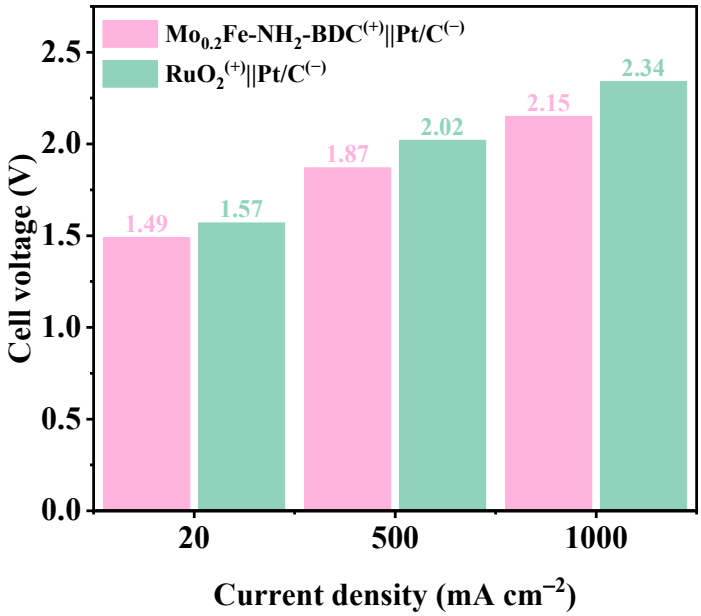

Fig. S9. Comparison of cell voltages required at varying current densities for $Mo_{0.2}Fe\text{-}NH_2\text{-}BDC^{(+)}$ || $Pt/C^{(-)}$ and $RuO_2^{(+)}$ || $Pt/C^{(-)}$ systems.

Table S1. Comparison of OER performances with previously reported catalysts in 1.0 M KOH solution.

Catalyst	Overpotential (mV)	Tafel slope (mV dec^{-1})	Reference
$Mo_{0.2}Fe$-NH_2-BDC	**254**	**66**	**This work**
Zr-Co_3O_4/NF	307	99	[1]
NiCo-HMT MOF/NF	330	86	[2]
$Dy_{0.05}$Fe-MOF/NF	258	82	[3]
Co-MOF/NF	270	75	[4]
CoCe-MOF/CP	267	96.1	[5]
$Ni_{0.5}Co_{1.5}$-bpy	256	81.8	[6]
CoS_x/Co-MOF	280	83	[7]
CoMo-MI-600	316	89.9	[8]
CoZnMOF/CC	287	76.3	[9]
Co-MOF-NK	268	77.5	[10]
Co-MOF-C	342	119	[11]
CoO_x-ZIF	320	70.3	[12]
MCCF/NiMn-MOFs	280	86	[13]
Co/Ni$(BDC)_2$TED	260	76.24	[14]
ZIF-67/CoNiAl-LDH/NF	303	88	[15]

Table S2. Overall water splitting performances of different catalysts in 1.0 M KOH solution.

Catalyst	Voltage (mA cm^{-2})	Reference
This work	**1.58/100**	**This work**
FeCu–BTC/WO_3–WC	1.73/100	[16]
NiMo/Ni-NDC	1.56/20	[17]
Ru@CoFe/D-MOFs	1.56/10	[18]
NCS/Ni-BDC	1.58/10	[19]
FeNi(BDC)(DMF,F)	1.58/10	[20]
$Co_{0.45}Fe_{0.45}Ni_{0.9}$-MOF/NF	1.59/10	[21]
Fe_2V-MOF	1.6/10	[22]
Fe-MOF@(Co,Ni)Fe-LDH	1.62/10	[23]
CdFe-BDC	1.68/10	[24]

References

1. G. Yang, B. Zhu, Y. Fu, J. Zhao, Y. Lin, D. Gao and J. Li, *J. Alloys Compd.*, 2021, **886**, 161172.
2. R. Zahid, M. R. Abdul Karim, F. S. Khan and M. A. Marwat, *RSC Adv.*, 2024, **14**, 13837-13849.
3. Y. Ma, G.-M. Mu, Y.-J. Miao, D.-M. Lin, C.-G. Xu, F.-Y. Xie and W. Zeng, *Rare Met.*, 2022, **41**, 844-850.
4. C.-P. Wang, H.-Y. Liu, G. Bian, X. Gao, S. Zhao, Y. Kang, J. Zhu and X.-H. Bu, *Small*, 2019, **15**, 1906086.
5. Y. Liao, Y. Xiao, Z. Li, X. Zhou, J. Liu, F. Guo, J. Li and Y. Li, *Small*, 2024, **20**, 2307685.
6. Y. Bai, G. Zhang, S. Zheng, Q. Li, H. Pang and Q. Xu, *Sci. China Mater.*, 2021, **64**, 137-148.
7. H. Xu, K. Ye, K. Zhu, J. Yin, J. Yan, G. Wang and D. Cao, *Inorg. Chem. Front.*, 2020, **7**, 2602-2610.
8. Y. Guo, Q. Huang, J. Ding, L. Zhong, T.-T. Li, J. Pan, Y. Hu, J. Qian and S. Huang, *Int. J. Hydrogen Energy*, 2021, **46**, 22268-22276.
9. J. Wu, Z. Yu, Y. Zhang, S. Niu, J. Zhao, S. Li and P. Xu, *Small*, 2021, **17**, 2105150.
10. M. Liu, L. Kong, X. Wang, J. He, J. Zhang, J. Zhu and X.-H. Bu, *Nano Res.*, 2021, **14**, 4680-4688.
11. J. Du, F. Zhang, L. Jiang, Z. Guo and H. Song, *Inorg. Chem. Commun.*, 2023, **158**, 111661.
12. S. Dou, C.-L. Dong, Z. Hu, Y.-C. Huang, J.-l. Chen, L. Tao, D. Yan, D. Chen, S. Shen, S. Chou and S. Wang, *Adv. Funct. Mater.*, 2017, **27**, 1702546.
13. W. Cheng, X. F. Lu, D. Luan and X. W. Lou, *Angew. Chem. Int. Ed.*, 2020, **59**, 18234-18239.
14. D.-J. Li, Q.-H. Li, Z.-G. Gu and J. Zhang, *J. Mater. Chem. A*, 2019, **7**, 18519-18528.

15. J. Xu, Y. Zhao, M. Li, G. Fan, L. Yang and F. Li, *Electrochim. Acta*, 2019, **307**, 275-284.
16. D. R. Paudel, U. N. Pan, R. B. Ghising, M. R. Kandel, S. Prabhakaran, D. H. Kim, N. H. Kim and J. H. Lee, *Appl. Catal. B Environ. Energy*, 2023, **331**, 122711.
17. M. K. Lee, S. Choi, H. Park, T. H. Lee, S. A. Lee, J. W. Yang, S. G. Ji, W. S. Cheon, S. H. Ahn, S. Y. Kim, M. Shokouhimehr, J. Y. Kim and H. W. Jang, *Energy Technol.*, 2023, **11**, 2201203.
18. D. Liu, C. Wang, Z. Zhou, C. Ye, R. Yu, C. Wang and Y. Du, *Inorg. Chem. Front.*, 2022, **9**, 6158-6166.
19. E. Sadeghi, N. S. Peighambardoust, S. Chamani and U. Aydemir, *ACS Mater. Au*, 2023, **3**, 143-163.
20. H.-W. Lin, D. Senthil Raja, X.-F. Chuah, C.-T. Hsieh, Y.-A. Chen and S.-Y. Lu, *Appl. Catal. B Environ. Energy*, 2019, **258**, 118023.
21. Y. Liu, P. Li, Z. Wang and L. Gao, *Materials*, 2024, **17**, 2195.
22. Y. Kong, D. Xiong, C. Lu, J. Wang, T. Liu, S. Ying, X. Ma and F.-Y. Yi, *ACS Appl. Mater. Interfaces*, 2022, **14**, 37804-37813.
23. L. Chen, Y. Luo, Z.-P. Yu, Y.-K. Cheng, Y. Zheng, L. He, J.-H. Xiong and W.-W. Kong, *Tungsten*, 2024, **6**, 859-868.
24. Y. Luo, X. Yang, L. He, Y. Zheng, J. Pang, L. Wang, R. Jiang, J. Hou, X. Guo and L. Chen, *ACS Appl. Mater. Interfaces*, 2022, **14**, 46374-46385.